



**HAL**  
open science

# Tuning the electrode activity to expose transformational and electrocatalytic characteristics of individual nanoparticles by nanoimpact electrochemistry

Nikolaos Kostopoulos, Mathias Miranda Vieira, Louis Godeffroy, Jérôme Médard, Catherine Combellas, Jean-francois Lemineur, Frédéric Kanoufi, Jean-marc Noël

## ► To cite this version:

Nikolaos Kostopoulos, Mathias Miranda Vieira, Louis Godeffroy, Jérôme Médard, Catherine Combellas, et al.. Tuning the electrode activity to expose transformational and electrocatalytic characteristics of individual nanoparticles by nanoimpact electrochemistry. *ChemElectroChem*, 2022, 9 (18), pp.57-82. 10.1002/celec.202200582 . hal-03816542

**HAL Id: hal-03816542**

**<https://hal.science/hal-03816542v1>**

Submitted on 16 Oct 2022

**HAL** is a multi-disciplinary open access archive for the deposit and dissemination of scientific research documents, whether they are published or not. The documents may come from teaching and research institutions in France or abroad, or from public or private research centers.

L'archive ouverte pluridisciplinaire **HAL**, est destinée au dépôt et à la diffusion de documents scientifiques de niveau recherche, publiés ou non, émanant des établissements d'enseignement et de recherche français ou étrangers, des laboratoires publics ou privés.

# Tuning the electrode activity to expose transformational and electrocatalytic characteristics of individual nanoparticles by nanoimpact electrochemistry.

Nikolaos Kostopoulos, Mathias Miranda Vieira, Louis Godeffroy, Jérôme Médard, Catherine Combellas, Jean-Francois Lemineur, Frederic Kanoufi,\* Jean-Marc Noël\*

This article is dedicated to the 65<sup>th</sup> anniversary of Hubert Girault

Dr. N. Kostopoulos, Dr. M. Miranda Vieira, L. Godeffroy, J. Médard, Dr. C. Combellas, Dr. J.-F. Lemineur, Dr. F. Kanoufi, Dr. J.-M. Noël  
ITODYS laboratory, CNRS,  
Université Paris Cité,  
F-750013 Paris, France.  
E-mail: frederic.kanoufi@u-paris.fr  
E-mail: jean-marc.noel@cnrs.fr

Supporting information for this article is given via a link at the end of the document.

**Abstract:** Nanoimpact electrochemistry (NIE) is a straightforward analytical technique to study at high throughput the reactivity of single Nanoparticles (NPs) colliding with a biased UltraMicroElectrode (UME). As NIE can reveal both NP size and catalytic activity, this strategy can be employed to establish relationships between these two NP descriptors. Herein, it is shown that the electrode material is crucial for visualizing simultaneously electro-catalytic processes and NP transformation, that can size the NPs. UMEs made of gold (Au) or glassy carbon (GC), were employed to study the reduction of AgBr NPs and the electrocatalytic activity of the resulting Ag NPs for the oxygen reduction reaction (ORR). With Au UME, only the transformation process is probed, allowing a quantitative analysis of the overpotential effect on the reduction dynamic of the AgBr NPs. When a GC UME is employed, the AgBr NPs reduction and subsequent ORR activity can be quantified for the very same NPs.

## Introduction

Nanoimpact electrochemistry (NIE), which was introduced more than a decade ago,<sup>[1,2]</sup> constitutes a straightforward analytical technique to study, at high throughput, single nano-objects and particularly nanoparticles (NPs).<sup>[3-9]</sup> In most cases, such experiments are carried out using an ultramicroelectrode (UME) immersed in a suspension of colloidal NPs. The analysis of the current spikes (shape and amplitude) arising from the collisions of individual NPs with the biased UME allows extracting valuable information about the colloidal system under investigation.

On the one hand, the NIE approach was employed to characterize NP transformation or dissolution processes. In the latter case, the electrochemical transients which are generally current spikes provide dynamic sizing<sup>[10]</sup> of the different populations<sup>[11]</sup> of NPs during their contact with the electrode surface. This allows deciphering several mechanistic aspects,<sup>[4,12]</sup> such as demonstrating the role of the potential applied to the electrode on the transformation rate,<sup>[12]</sup> the possible occurrence of multistep reactions during NP transformation,<sup>[13-19]</sup> as well as the importance of electrostatic

forces,<sup>[20,21]</sup> electrolyte concentration,<sup>[22]</sup> NPs-electrode interactions<sup>[11,23]</sup> or NPs motion.<sup>[18,19,24]</sup>

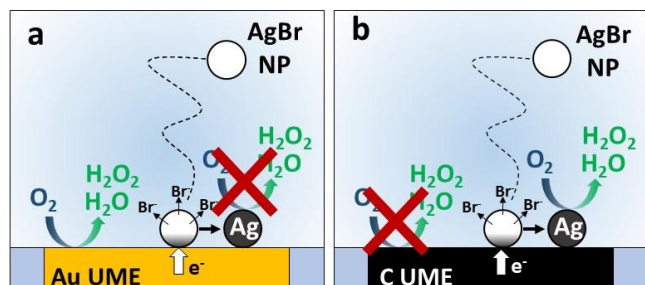
On the other hand, NIE was employed to determine the electrocatalytic activity of individual NPs. Many electrocatalytic reactions have been inspected including the oxygen evolution,<sup>[25,26]</sup> or reduction,<sup>[27,28]</sup> hydrogen evolution,<sup>[29-33]</sup> or oxidation,<sup>[34]</sup> hydrogen peroxide oxidation<sup>[35]</sup> and reduction,<sup>[36]</sup> and hydrazine oxidation reactions.<sup>[37-39]</sup> Besides, these reactions were inspected at a variety of NPs such as metals (Pd,<sup>[29]</sup> Pt,<sup>[27,30,34,36,37,39]</sup> Au,<sup>[30,31]</sup>), metal oxides (CoFe<sub>2</sub>O<sub>4</sub>,<sup>[25]</sup> IrO<sub>x</sub>,<sup>[35]</sup> Pt@TiO<sub>2</sub>,<sup>[28]</sup> Ni(OH)<sub>2</sub><sup>[40]</sup>) or carbon materials.<sup>[24,41,42]</sup> The electrocatalytic activity of a NP is detected by an abrupt increase of the current, the height of which reflects the electrocatalytic efficiency, the dynamics (passivation, etc...)<sup>[30]</sup> at the single NP level,<sup>[29]</sup> or the NP active area.<sup>[38]</sup>

Herein, we take advantage of a transformation/electrocatalytic NIE strategy, previously employed to study the transformation of Ag NPs to Ag<sub>2</sub>O followed by their electrocatalytic activity for the OER.<sup>[26]</sup> We selected AgBr NPs as a model system that represent easy to use precursors of metal Ag NPs, widely studied by NIE.<sup>[4]</sup> Indeed, Ag NPs can be readily obtained by the reduction of AgBr NPs (Equation 1) and display a good electrocatalytic activity for the ORR in neutral pH aqueous media (equation 2).<sup>[43]</sup>



In particular, following Sepunaru's recent work,<sup>[32]</sup> the collisions of NPs were recorded at different electrode materials (catalytically inactive or active). Even if most NIE studies are performed at catalytically inactive electrodes in order to inspect the catalytic activity of the NP, Sepunaru demonstrated that the catalytic activity of the NPs was annihilated at catalytically active electrodes as no electrochemical collisions was detected. By varying the activity of the electrode, deeper mechanistic insights were reached regarding the electrocatalysis at the NP.<sup>[32]</sup> Herein, we will use a catalytically active electrode (Au UME) to suppress

the catalytic response of the NPs and therefore to study their redox transformation (Scheme 1a). Alternatively, a catalytically inactive electrode (C UME) will allow probing both the transformation and the electrocatalytic activity of the NPs (Scheme 1b).



Scheme 1. NIE mechanism occurring at a) the Au UME and b) the C UME.

## Results and Discussion

Firstly, the electrocatalytic properties of the electrode materials for the ORR were inspected and compared to that of Ag. Figure 1a shows the linear sweep voltammograms recorded at Au, Ag and C UMEs, in aerated electrolytic solutions. All UMEs show a reductive wave characteristic of the ORR, but with overpotentials increasing in the order Au < Ag < C.

Since Ag has intermediate electrocatalytic activity compared to Au and C, it is pertinent investigating the reduction of AgBr NPs on both Au and Glassy carbon (GC) UMEs. Before apprehending the reductive behavior of AgBr NPs at the single level by NIE experiments, a large ensemble of NPs immobilized on an UME was studied. Figure 1b presents the cyclic voltammogram recorded at the Au UME modified with dropcasted AgBr NPs. On the forward reductive scan, a first cathodic peak at -0.32V (associated to a backward reoxidation at -0.20V) is assigned to the reduction of AgBr to Ag (equation 1). The backward reoxidation peak corresponds to the reoxidation of Ag to AgBr, owing to the 0.1M Br<sup>-</sup> containing electrolyte. This system is followed by the ORR reaction indicating that the AgBr to Ag conversion occurs at potentials ~ 0.3V more positive than the ORR and that both electrochemical reactions (AgBr to Ag conversion and ORR) can be decomposed when analysing the system at different electrode potentials.

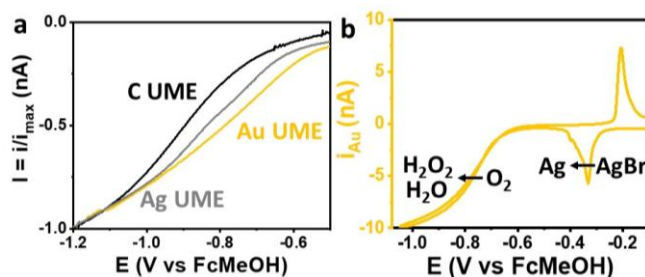


Figure 1. a) Normalized linear sweep voltammograms on gold (yellow trace), silver (grey line), and carbon (black line) UMEs. b) Cyclic voltammogram of Au UME modified with dropcasted AgBr NPs. All measurements are recorded vs FcMeOH in air saturated aqueous solutions of 0.1 M KBr at 50 mV/s.

Then the AgBr NPs electrochemical behaviour is investigated at the single NP level by immersing Au or C UMEs in a freshly prepared colloidal suspension of AgBr NPs (protocol detailed in the experimental section) diluted 10 times.

The current transients recorded at the Au UME at various potentials ranging from -0.6 to -1.5 V vs FcMeOH are shown in Figure 2a. All transients display current spikes, such as the one presented in the inset of Figure 2b which was recorded at -0.9 V vs FcMeOH. Other examples provided in Figure S1 show the same behaviour. According to Figure 1b, within this potential range, those spikes can be confidently attributed to the reduction of AgBr to Ag (equation 1). One can also observe in Figure 2c and 2d an increase of the individual current spikes' amplitude when the UME potential becomes more negative, whereas the spikes' duration decreases. Similar effect reported previously while increasing the overpotential of Ag NPs oxidation,<sup>[12]</sup> was attributed to the increase of the transformation kinetic of NPs with the overpotential. Applying more negative potentials is also accompanied by a continuous increase of the impact frequency until -1.4 V vs FcMeOH as shown in Figure S2. This could be due to electrochemically driven phoretic processes (favoured at increased electrochemical current, here more negative potentials), resulting in an apparent acceleration and preconcentration of the NPs in the vicinity of the electrode.<sup>[44]</sup> However, despite changes in characteristic amplitude and duration the total charge of the spikes remains statistically the same in the entire potential range, as shown in Figure 2e, attesting that the same NP population are probed at the different electrode potentials. Considering that the ORR is catalyzed preferentially on the electrocatalytically active Au surface, this likely means that this ORR reaction is prevented at the NPs' surface so that the current spikes observed solely correspond to the reduction of the AgBr NPs to Ag<sup>[17]</sup> according to equation 1. This is corroborated by the quasi-steady-state background current,  $i_{bg, Au}$  recorded during the NIE. As the potential applied at the Au UME decreases,  $i_{bg, Au}$  becomes more negative, following a sigmoidal evolution similar to that of the voltammogram of Figure 1a, with a similar apparent half-wave potential  $E_{app, Au UME}^0 \sim -0.75$  V vs FcMeOH as shown in Figure 3a. The evolution of  $i_{bg, Au}$  with the Au UME potential therefore corresponds to the extent of the ORR occurring at the Au UME during the NIE experiments.

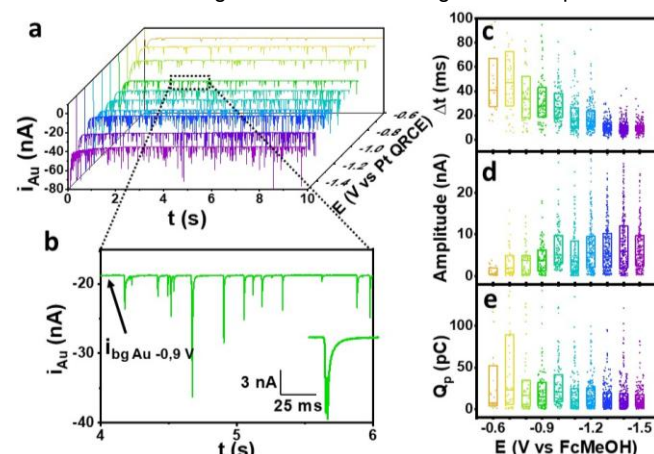


Figure 2. a) Transients of NIE experiments in a colloidal suspension of AgBr NPs occurring on gold UME in air saturated aqueous mixtures containing 0.1 M KCl, recorded from -0.6 V to -1.5 V vs FcMeOH, every 100 mV and b) zoom of the chronoamperogram recorded at -0.9 V vs FcMeOH. Evolution of the c) duration, d) amplitude and e) charge,  $Q_p$ , (peak area) for the current spikes extracted from Figure 2a.

The current transients recorded at the C UME for the same range of potentials (-0.6 V to -1.5 V vs FcMeOH) are provided in Figure S3. As observed with the Au UME and illustrated in

Figures S3 and S4, when the C UME potential becomes more negative the current spikes' amplitude and frequency increase, their duration decrease whereas the global charge remains the same. By analogy, these current spikes can be attributed to the conversion of the AgBr NPs into Ag NPs.

However, looking carefully at all the transients of Figure S3, specific features can be observed within a range of  $E_{C\ UME}$  from -0.6 V to -1.0 V vs FcMeOH. As exemplified in the transient of Figure 3b for a potential of -0.9 V, the 'conversion' current spikes (Figure 3c) are eventually followed by current steps (Figure 3d). The upside-down histogram of Figure 3a represents the probability to observe a current step right after a 'conversion' current spike at the C UME with a limit of detection of  $\sim 10$  pA and for a number of analyzed current spikes  $N > 20$  for each potential. On one hand, the probability of observing such current step event after the conversion increases from -0.6 V and reaches a maximum of  $\sim 85\%$  at -0.9 V. The Figure 3a (Black curve) also displays the evolution with potential of the background current,  $i_{bg\ C}$  at the C UME extracted from Figure S3. It shows that within the range -0.6 V to -0.9 V the background ORR current recorded at the C UME remains very low. However, since Ag is able to catalyse the ORR within this range of potential (based on the voltammogram at the Ag UME, Figure 1a), the current steps are attributed to the electrocatalytic ORR into  $H_2O$  or  $H_2O_2$  (Equation 2 or 3, respectively) at the just-electrochemically converted Ag NPs.<sup>[27]</sup> Interestingly, the 'catalytic' steps probability increase when increasing the overpotential from -0.6 to -0.9 V, following the electrocatalytic activity of the Ag UME: the more negative the potential, the higher the ORR activity at the electrochemically generated Ag NPs. This observation is in line with those reported previously for the oxidation of Ag to  $Ag_2O$  followed by the OER.<sup>[26]</sup>

For  $E_{C\ UME} < -0.9$  V the abrupt decrease of the probability is associated to the increase of  $i_{bg}$  recorded at the C UME (Figure 3a, black curve) that give an apparent half-wave potential for the ORR of  $E_{app\ C\ UME}^0 \sim -0.95$  V vs FcMeOH consistent with the voltammogram of Figure 1a. It ends up with the complete disappearance of the current steps at  $E_{C\ UME} < -1.1$  V (see for instance in Figure S4 at -1.2 V) a potential corresponding to the current plateau of the ORR at the C UME. At this potential value, the Ag NPs are electrogenerated at the UME in a region devoid of  $O_2$ , preventing the observation (actually decreasing the extent) of ORR at the catalytic Ag NP. In this potential region, the individual current spikes observed on the chronoamperometric traces are similar to those observed on the Au UME (Figure S1). This suggests that when the ORR is taking place at the C UME, only the AgBr NP reductive conversion to Ag, Equation 1, is detected by the NIE, the C UME acting as a reactive electrode.<sup>[32]</sup>

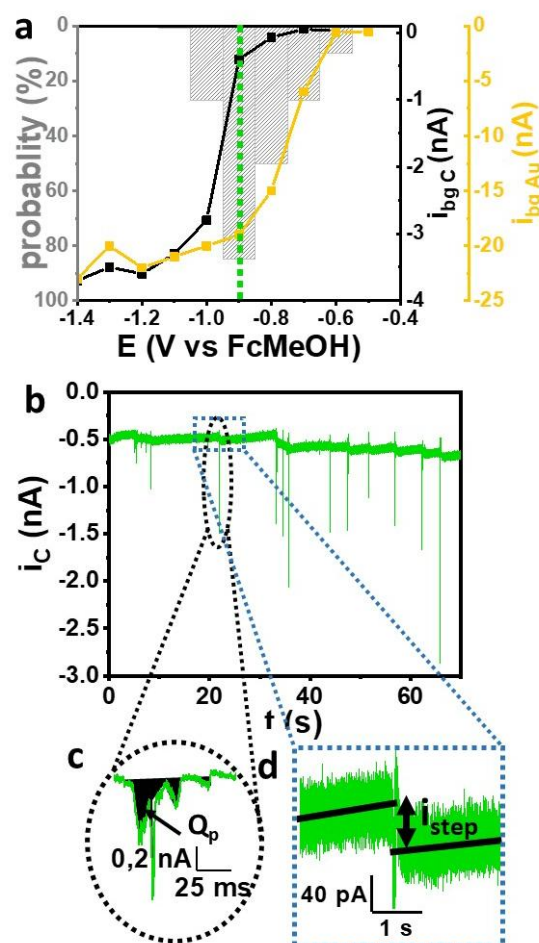


**Figure 3.** a) background currents,  $i_{bg}$ , recorded at various potential (from -0.6 V to -1.5 V vs FcMeOH) on a 25  $\mu m$  Au UME (yellow) and a 7  $\mu m$  GC UME (black) immersed in a solution of AgBr NPs diluted 10 times and histogram showing the probability to observe current steps after the current spikes at each potential b) Transient recorded at -0.9 V vs FcMeOH at a GC UME in a solution of AgBr NPs diluted 10 times and c) zoom of a single AgBr NP reduction spike and d) its corresponding current step characteristic of the ORR at reduced AgBr to Ag NPs.

Since the NIE experiments performed using the Au UME were free of electrocatalytic behavior, they were further employed to investigate the potential dependence of the AgBr NPs' conversion process. A statistical analysis of all the current spikes was performed at each potential. The charge  $Q_p$  of each spike associated to this conversion is used to estimate the size of the NP colliding the UME. The apparent electrochemical radius,  $r_{EC}$ , of the AgBr NP is extracted from equation 4:

$$r_{EC} = \sqrt[3]{\frac{3Q_p M}{4\pi F \rho}} \quad (4)$$

with  $M$  and  $\rho$  the molar mass and density of AgBr, respectively,  $F$  the Faraday constant. The values of the equivalent radius,  $r_{EC\ Au}$ , for all Au UME potentials are plotted along its corresponding conversion duration,  $\Delta t$ , in Figure 4a. As previously reported for mixtures of AgX NPs ( $X=Br$  or  $Cl$ )<sup>[17]</sup>  $r_{EC\ Au}$  varies linearly with  $\Delta t$ . Herein, this holds true for each UME potential (each color in Figure 4a) with an increase of the slope when the potential decreases. Examples of such linear relationships are detailed in Figure S5. This observation is associated with the shortening of the peak duration with decreasing the UME potential. As shown in Figure 2c,  $\Delta t$

decreases from 50-60 ms at -0.6 V down to <20 ms at -1.5 V. This suggests that the kinetics of AgBr reduction depends on its overpotential. This is consistent with previous observations reported for the reverse reaction *i.e.*, the oxidation of Ag NPs to AgCl NPs.<sup>[25]</sup>

Noteworthy, the linear variation of  $\Delta t$  with NP size questions a diffusion-limited transformation process which would predict a parabolic evolution,  $\Delta t = r_{EC}^2/D_{Ag^+}$ .<sup>[17]</sup> Moreover, for a 100 nm diameter AgBr NP with  $D_{Ag^+} \sim 10^{-11} \text{ cm}^2 \cdot \text{s}^{-1}$  (which is the diffusion coefficient of  $\text{Ag}^+$  within solid AgBr<sup>[45]</sup>), the diffusion-limited conversion process would take  $\Delta t \approx 2.5 \text{ s}$ . This duration is about two orders of magnitude higher than the ones observed in the present study. Additionally, a limitation by the diffusion of  $\text{Br}^-$  can be ruled out since with a  $D_{\text{Br}^-}$  in AgBr one order of magnitude lower than in solution ( $D_{\text{Br}^-} \sim 6 \times 10^{-7} \text{ cm}^2 \cdot \text{s}^{-1}$ )<sup>[46]</sup> one would expect  $\Delta t$  in the order of the  $\mu\text{s}$ . Altogether, this suggests that for such large NPs, the AgBr conversion is not limited by the sole diffusion of ions in the ionic crystal matrix. It was previously shown that the NP transformation could be modeled as the formation of a new solid (metallic Ag) phase expanding at the expense of the AgBr phase.<sup>[17,47]</sup> The conversion is suggested to occur at the moving boundary between the Ag and the AgBr phases. The observations in the present study, introduce a new kinetic regime for such interfacial conversion equivalent to the hopping of an electron ( $e_{\text{Ag}}$ ) from reduced  $\text{Ag}_{\text{red}}$  sites to adjacent unreduced AgBr sites within the NP.<sup>[17,47]</sup> Herein, this is schematized by equation 5.

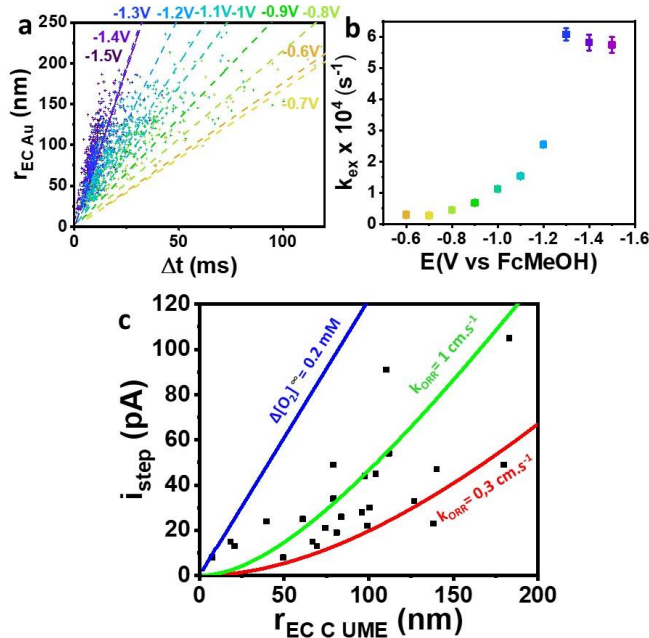
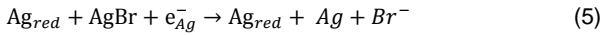


**Figure 4.** a) Electrochemical radius of the NPs, extracted from  $Q_p$ , plotted versus their duration, with best linear trendline for each potential from which b) hopping rate constant,  $k_{\text{ex}}$ , extracted for each Au UME potential (details in text). c) current steps plotted versus their corresponding electrochemical NP radius ( $r_{\text{EC}}$ ) extracted from transients of Figure 3b and others recorded at -0.9V at the C UME with the trendlines for the upper-limit mass-transfer regime (blue) and for kinetic limitation from the ORR with  $k_{\text{ORR}} = 0.3 \text{ cm} \cdot \text{s}^{-1}$  (red) and  $1 \text{ cm} \cdot \text{s}^{-1}$  (green).

The conversion dynamics is then characterized by both the diffusion of ions in the ionic solid phase and the hopping rate

constant  $k_{\text{ex}}$  (in  $\text{s}^{-1}$ ) depicting equation 5. A COMSOL model of this situation, previously presented,<sup>[17,47]</sup> confirmed the linear relationship between the conversion duration,  $\Delta t$ , and the NP radius,  $r_{\text{EC}}$  and  $\Delta t$  following the analytical expression given by equation 6.

$$r_{\text{EC}} = 10^7 \sqrt{D_{\text{Ag}^+} k_{\text{ex}}} \Delta t \quad (6)$$

with  $r_{\text{EC}}$  expressed in nm,  $D_{\text{Ag}^+}$  in  $\text{cm}^2 \cdot \text{s}^{-1}$ ,  $k_{\text{ex}}$  in  $\text{s}^{-1}$  and  $\Delta t$  in s. The evolution of  $k_{\text{ex}}$  with the UME potential, (Figure 4b) shows that  $k_{\text{ex}}$  increases with the potential up to a limit  $k_{\text{ex,max}} \sim 6 \times 10^4 \text{ s}^{-1}$  at  $E_{\text{C UME}} = -1.3 \text{ V}$  vs FcMeOH. This value is one order of magnitude lower than the highest interatomic exchange diffusion limit  $k_{\text{ex,lim}} \sim 6 \times 10^5 \text{ s}^{-1}$  determined from the Smoluchovsky theory (Equation 7):

$$k_{\text{ex,lim}} = \frac{8\pi D_{\text{Ag}^+} a N_A}{\rho} \quad (7)$$

with  $N_A$  the Avogadro number and  $a = 3.5 \text{ \AA}$ , the interatomic distance in the AgBr crystal. It is noteworthy that if one assumes that the maximum value estimated experimentally corresponds to the Smoluchovsky diffusion limit (Equation 7), then equating the expression of  $k_{\text{ex,lim}}$  with that for the evaluation of  $k_{\text{ex,max}}$ , respectively from Equations 6 and 7, yields a diffusion of ions in the AgBr crystal of the order of  $D_{\text{Ag}^+} \sim 3 \cdot 10^{-12} \text{ cm}^2 \cdot \text{s}^{-1}$ . This value is in reasonable agreement with the literature one. It further highlights that the high temporal resolution of NIE allows inspecting diffusion-limited hopping mechanism in solid NPs.

Finally, the electrocatalytic activity for the ORR at the reduced AgBr NPs was quantitatively investigated using the C UME. A series of spikes followed by a current step recorded at -0.9 V vs FcMeOH at a GC UME extracted from Figure 3b and others were analyzed. The transients recorded at this specific potential present the highest probability to observe an electrocatalytic current step after a current spike (Figure 3a). Each current step,  $i_{\text{step}}$  was then related to the charge of the preceding current spike  $Q_p$ , as illustrated in Figure 3c and 3d, respectively. The current spikes often occur through multiple spike events as shown in Figure 3d, within a < 50 ms range. Such behavior is characteristic of a reduction proceeding through multiple NP-electrode contact events as observed for other Ag-based NPs.<sup>[13-19]</sup>

In a first approach, the multiple current spikes were considered as a unique transformation process, from which the NP radius  $r_{\text{EC}}$  was evaluated using Equation 4, and the current step considered as the electrocatalytic activity for the ORR. This approximation is further supported by the fact that the spike charges are statistically similar to those observed when the electrocatalytic activity of the NPs is hindered *i.e.*, (1) on the catalytically active Au UME whatever its polarization, or (2) at the C UME for  $E_{\text{C UME}} < -1.1 \text{ V}$  vs FcMeOH (Figure S3).

Figure 4c shows the plot of  $i_{\text{step}}$  versus  $r_{\text{EC}}$  for a statistically representative number of events. Assuming that the ORR activity of the NPs is limited by the mass transfer of  $\text{O}_2$ , the current step should be directly proportional to the electrochemical radius,  $r_{\text{EC}}$  following equation 8.<sup>[38,39,48]</sup>

$$i_{\text{step}} = 4\pi n F D_{\text{O}_2} \Delta[\text{O}_2] r_{\text{EC}} \quad (8)$$

where  $n=3.3$  is the number of electrons exchanged for the ORR at Ag,<sup>[43]</sup>  $F$  is the Faradaic constant,  $D_{O_2} \sim 2 \times 10^{-5} \text{ cm}^2 \cdot \text{s}^{-1}$  is the diffusion coefficient for  $O_2$  in water,  $\Delta[O_2] = [O_2]^{\infty} - [O_2]_{NP}$  is the concentration difference between the bulk solution and the NP surface, which is at maximum  $\sim 0.25 \text{ mM}$  in air-saturated aqueous solution.

On the other hand, a kinetic limitation from the ORR, with a rate constant  $k_{ORR}$ , at the NP surface would be described by a quadratic Butler-Volmer expression:

$$i_{step} = 4\pi n F r_{EC}^2 k_{ORR} [O_2]_{NP} \quad (9)$$

Combined with the mass transfer arrival of  $O_2$  at the NP, from Equation 8, one would expect the ORR electrocatalysis current follows Equation 10:

$$i_{step} = \frac{4\pi n F r_{EC}^2 k_{ORR} [O_2]_{NP}}{1 + \frac{k_{ORR} r_{EC}}{D_{O_2} n z}} \quad (10)$$

This equation should allow analyzing the ORR kinetic at the single NP and apprehend kinetic vs mass transfer competition with NP size.

Along with the scatter plot in Figure 4d are provided the maximal mass-transfer limited linear trend (Equation 8) and two kinetically-limited trends evaluated, using Equation 10, for  $k_{ORR} = 0.3$  and  $1 \text{ cm s}^{-1}$  respectively.

Noteworthy, the upper-limit mass-transfer regime was evaluated considering that  $\sim 20\%$  of  $O_2$  is consumed by the C UME (extracted from  $i_{bg,C}$  at  $-0.9 \text{ V}$  vs FcMeOH in Figure 3a). It means that the NP would probe at best an apparent bulk concentration  $\Delta[O_2] = 0.8[O_2]^{\infty} = 0.2 \text{ mM}$ .

Despite the scatter in the data which might be explained by the disparity of the NPs catalytic efficiency the current steps are within the predicted mass-transfer and kinetic currents. It suggests that the ORR kinetic at the Ag NPs is higher than  $0.3 \text{ cm s}^{-1}$ . The scatter in the data could further suggest a size effect on the ORR kinetics with increasing activity when the NP size decreases.

## Conclusion

The nanoimpact electrochemistry (NIE) approach was implemented to shed light on the reduction of AgBr NPs to Ag on gold and carbon ultramicroelectrodes. On both electrodes, typical current spikes of AgBr NPs reduction to Ag NP were observed, whereas specifically on the C UME for a potential window between  $-0.6 \text{ V}$  to  $-1.0 \text{ V}$ , the AgBr NPs transformation was accompanied by current steps. The latter, attributed to the electrocatalytic ORR at individual electrogenerated Ag NPs, exhibit the highest probability of occurrence at  $-0.9 \text{ V}$ . Conversely, when the ORR takes place at the surface of the catalytically active Au UME, a gradient of the molecular reactant's concentration is imposed in the vicinity of the UME, hindering the catalytic reaction at the Ag NPs. Hence, for NPs less active than the UME itself (here  $\text{Ag} < \text{Au}$ ), electrocatalysis of the ORR at the NP cannot be detected whatever the potential applied at the UME. By hindering the ORR at the NP, the dynamics of the reductive conversion of AgBr NPs to Ag was

analyzed. The reduction is characterized by a hopping mechanism, associated to an advancing Ag/AgBr boundary within the NP during its conversion. The hopping electron transfer rate constant within the AgBr NPs increases with a more cathodic potential until it reaches a limit at  $-1.2 \text{ V}$ , suggesting a further limitation of the reduction process. In addition, by employing a C UME, the ORR activity extracted from the current steps was compared to the NPs' size defined from the corresponding current spikes. The trends observed suggest ORR in a mixed control by mass transfer and ORR activity with a lower-bound electrocatalysis rate of  $0.3 \text{ cm s}^{-1}$ . This double NIE approach opens the way towards the determination of size-activity relationships that was recently reported as a possible explanation for heterogeneous electrocatalytic activities of Pd NPs during NIE experiments.<sup>[29]</sup>

## Experimental Section

### AgBr NPs synthesis

Analytical grade chemicals were obtained from Sigma-Aldrich and were used without further purification. Solutions were prepared with ultrapure water with a resistivity higher than  $18.2 \text{ M}\Omega \cdot \text{cm}$ . AgBr NPs were synthesized according to a previously described procedure<sup>[17,47]</sup> with minor changes.  $1 \text{ mL}$  of KBr solution ( $0.5 \text{ M}$ ) was mixed with  $98 \text{ mL}$  of cetyltrimethylammonium bromide solution ( $2 \text{ mM}$ ). Then,  $1 \text{ mL}$  of  $\text{AgNO}_3$  solution ( $0.5 \text{ M}$ ) was added dropwise and under constant stirring to form a  $100 \text{ mL}$  stock solution. The mixture was further stirred at room temperature for  $3 \text{ h}$  and became cloudy and white.

The colloidal solution was stored under light protection at  $4 \text{ }^\circ\text{C}$  until use in NIE. The AgBr NPs were analysed by SEM-EDX (Figure S6) using a Gemini 360 SEM from Zeiss coupled to an energy-dispersive X-ray detector from Oxford Instruments. The acceleration voltage was equal to  $8 \text{ kV}$ . For EDX analysis, the microscope aperture size was expanded from  $30$  to  $60 \text{ }\mu\text{m}$ . EDX data were processed using the Aztec software. The size distribution of the NPs determined from the SEM images is in fairly good agreement with the one extracted from the NIE experiments performed at the C UME (Figure S6).

### UME preparation

Homemade UMES were designed using borosilicate glass capillaries (Sutter instruments, Novato, California) with outer and inner diameters of  $1.0$  and  $0.5 \text{ mm}$ , respectively.  $25 \text{ }\mu\text{m}$  diameter gold wires or  $7 \text{ }\mu\text{m}$  carbon fiber ( $99.99\%$ , Goodfellow, Cambridge Ltd, Huntingdon, England) were inserted into the capillaries and sealed with a laser pipette puller (Sutter Instruments, Model PC-10, London, UK). The UMES were then polished with aluminum oxide tape ( $3 \text{ }\mu\text{m}$  from Precision Surfaces International, Houston, Texas, USA).

### NIE experiments

The stochastic EC collisions of NPs were recorded in a 2-electrode system using either the C or the Au UME as the working electrode and a Pt wire as both counter and pseudo-reference electrode. Current transients were recorded at  $10 \text{ kHz}$  bandwidth with a low noise current amplifier (Element eONE) and the  $10$  times diluted solution of AgBr NPs freshly synthesized. Noteworthy, the NIE experiments with the Au UME were performed with another batch of slightly larger AgBr NPs synthesized using the same procedure described above. To ensure a reliable comparison between the C and Au UME, all the potential values were referenced versus FcMeOH internal reference by adding into the solution  $1 \text{ mM}$  FcMeOH from Sigma-Aldrich after the NIE experiments (Figure S7).

## Acknowledgements ((optional))

We thank CNRS, the ANR JCJC program (PIRaNa project, ANR-20-CE42-0001) and the Emergence call from the Université de Paris within the Investissement d'Avenir program under reference ANR-18-IDEX-0001 for financial support. We also thank the Ile-de-France region and IDEX for financial support of the AFM-Beam-Rex platform

**Keywords:** Nanoimpact electrochemistry • Single Nanoparticle • electrocatalysis • Size-activity relationship • oxygen reduction reaction

- [1] X. Xiao, F.-R. F. Fan, J. Zhou, A. J. Bard, *J. Am. Chem. Soc.* **2008**, *130*, 16669.
- [2] Y.-G. Zhou, N. V. Rees, R. G. Compton, *Angewandte Chemie International Edition* **2011**, *50*, 4219.
- [3] Y. Y. Peng, R. C. Qian, M. E. Hafez, Y. T. Long, *ChemElectroChem* **2017**, *4*, 977.
- [4] P. A. Defnet, T. J. Anderson, B. Zhang, *Current Opinion in Electrochemistry* **2020**, *22*, 129.
- [5] K. J. Stevenson, K. Tschulik, *Current Opinion in Electrochemistry* **2017**, *6*, 38.
- [6] Y. Y. Peng, D. Guo, W. Ma, Y. T. Long, *ChemElectroChem* **2018**, *5*, 2982.
- [7] F. T. Patrice, K. Qiu, Y. L. Ying, Y. T. Long, *Annual Review of Analytical Chemistry* **2019**, *12*, 347.
- [8] S. M. Lu, J. F. Chen, Y. Y. Peng, W. Ma, H. Ma, H. F. Wang, P. Hu, Y. T. Long, *Journal of the American Chemical Society* **2021**, *143*, 12428.
- [9] L. K. Allerston, N. V. Rees, *Current Opinion in Electrochemistry* **2018**, *10*, 31.
- [10] M. Miranda Vieira, J. F. Lemineur, J. Médard, C. Combellas, F. Kanoufi, J. M. Noël, *Electrochemistry Communications* **2021**, *124*, 106950.
- [11] H. Ma, J.-F. Chen, H.-F. Wang, P.-J. Hu, W. Ma, Y.-T. Long, *Nature Communications* **2020**, *11*, 2307.
- [12] E. N. Saw, M. Kratz, K. Tschulik, *Nano Research* **2017**, *10*, 3680.
- [13] S. M. Oja, D. A. Robinson, N. J. Vittii, M. A. Edwards, Y. Liu, H. S. White, B. Zhang, *Journal of the American Chemical Society* **2017**, *139*, 708.
- [14] D. A. Robinson, M. A. Edwards, Y. Liu, H. Ren, H. S. White, *Journal of Physical Chemistry C* **2020**, *124*, 9068.
- [15] W. Ma, H. Ma, J. F. Chen, Y. Y. Peng, Z. Y. Yang, H. F. Wang, Y. L. Ying, H. Tian, Y. T. Long, *Chemical Science* **2017**, *8*, 1854.
- [16] J. Ustarroz, M. Kang, E. Bullions, P. R. Unwin, *Chemical Science* **2017**, *8*, 1841.
- [17] J.-F. Lemineur, J.-M. Noël, C. Combellas, F. Kanoufi, *Nanoscale* **2020**, *12*, 15128.
- [18] F. Zhang, M. A. Edwards, R. Hao, H. S. White, B. Zhang, *Journal of Physical Chemistry C* **2017**, *121*, 23564.
- [19] D. A. Robinson, Y. Liu, M. A. Edwards, N. J. Vittii, S. M. Oja, B. Zhang, H. S. White, *Journal of the American Chemical Society* **2017**, *139*, 16923.
- [20] M. Azimzadeh Sani, N. G. Pavlopoulos, S. Pezzotti, A. Serva, P. Cignoni, J. Linnemann, M. Salanne, M. Gaigeot, K. Tschulik, *Angewandte Chemie International Edition* **2021**, *2*.
- [21] E. N. Saw, K. Kanokkanchana, H. M. A. Amin, K. Tschulik, *ChemElectroChem* **2022**, *9*, 1.
- [22] K. J. Krause, F. Brings, J. Schnitker, E. Kätelhön, P. Rinklin, D. Mayer, R. G. Compton, S. G. Lemay, A. Offenhäusser, B. Wolfrum, *Chemistry - A European Journal* **2017**, *23*, 4638.
- [23] P. A. Defnet, B. Zhang, *Journal of the American Chemical Society* **2021**, *143*, 16154.
- [24] A. D. Pendergast, Z. Deng, F. Maroun, C. Renault, J. E. Dick, *ACS Nano* **2021**, *15*, 1250.
- [25] A. El Arrassi, Z. Liu, M. V. Evers, N. Blanc, G. Bendt, S. Saddeler, D. Tetzlaff, D. Pohl, C. Damm, S. Schulz, K. Tschulik, *Journal of the American Chemical Society* **2019**, *141*, 9197.
- [26] F. Zhang, P. A. Defnet, Y. Fan, R. Hao, B. Zhang, *Journal of Physical Chemistry C* **2018**, *122*, 6447.
- [27] Z. P. Xiang, A. D. Tan, Z. Y. Fu, J. H. Piao, Z. X. Liang, *Journal of Energy Chemistry* **2020**, *49*, 323.
- [28] Q. Wang, J. H. Bae, A. B. Nepomnyashchii, R. Jia, S. Zhang, M. V. Mirkin, *The Journal of Physical Chemistry Letters* **2020**, *11*, 2972.
- [29] M. Chen, S.-M. Lu, Y.-Y. Peng, Z. Ding, Y.-T. Long, *Chemistry - A European Journal* **2021**, *7*, 1.
- [30] Y. Y. Bai, Z. T. Feng, Y. J. Yang, X. Y. Yang, Z. L. Zhang, *Analytical Chemistry* **2022**, *94*, 1302.
- [31] M. Zhou, D. Wang, M. V. Mirkin, *ChemElectroChem* **2018**, *5*, 2991.
- [32] B. Roehrich, L. Sepunaru, *Angewandte Chemie - International Edition* **2020**, *59*, 19184.
- [33] P. A. Defnet, C. Han, B. Zhang, *Analytical Chemistry* **2019**, *91*, 4023.
- [34] X. Jiao, C. Lin, N. P. Young, C. Batchelor-McAuley, R. G. Compton, *Journal of Physical Chemistry C* **2016**, *120*, 13148.
- [35] M. Zhou, Y. Yu, K. Hu, H. L. Xin, M. V. Mirkin, *Analytical Chemistry* **2017**, *89*, 2880.
- [36] X. Chang, C. Batchelor-McAuley, R. G. Compton, *Chemical Science* **2020**, *11*, 4416.
- [37] T. M. Alligrant, R. Dasari, K. J. Stevenson, R. M. Crooks, *Langmuir* **2015**, *31*, 11724.
- [38] Y. Xiao, F. R. F. Fan, J. Zhou, A. J. Bard, *Journal of the American Chemical Society* **2008**, *130*, 16669.
- [39] S. J. Kwon, H. Zhou, F. R. F. Fan, V. Vorobyev, B. Zhang, A. J. Bard, *Physical Chemistry Chemical Physics* **2011**, *13*, 5394.
- [40] M. M. Vieira, J.-F. Lemineur, J. Médard, C. Combellas, F. Kanoufi, J. M. Noël, *Journal of Physical Chemistry Letters* **2022**, *13*, 5468.
- [41] Z. Deng, C. Renault, *Chemical Science* **2021**, *12*, 12494.
- [42] A. D. Pendergast, C. Renault, J. E. Dick, *Analytical Chemistry* **2021**, *93*, 2898.
- [43] Y. Guo, M. Yang, R. C. Xie, R. G. Compton, *Chemical Science* **2021**, *12*, 397.
- [44] A. N. Patel, A. Martinez-Marrades, V. Brasiliense, D. Koshelev, M. Besbes, R. Kuszelewicz, C. Combellas, G. Tessier, F. Kanoufi, *Nano Letters* **2015**, *15*, DOI 10.1021/acs.nanolett.5b02921.
- [45] C. Alonso, R. C. Salvarezza, J. M. Vara, A. J. Arvia, *Electrochimica Acta* **1990**, *35*, 489.
- [46] M. V. Mirkin, M. Arca, A. J. Bard, *Journal of Physical Chemistry* **1993**, *97*, 10790.
- [47] J.-F. Lemineur, J.-M. Noël, A. Courty, D. Ausserré, C. Combellas, F. Kanoufi, *Journal of the American Chemical Society* **2020**, *142*, 7937.
- [48] H. S. Ahn, A. J. Bard, *Angewandte Chemie - International Edition* **2015**, *54*, 13753.

